



OPEN Receptor mechanism producing a sweet taste from plant aroma compounds

Fuyumi Horie¹, Keisuke Sanematsu^{2,3,4}, Keiko Yasumatsu^{5,6}, Takatsugu Hirokawa^{7,8}, Noriatsu Shigemura^{2,4}, Atsuko Yamashita^{9,10} & Yuko Kusakabe^{1✉}

Fruits and vegetables contain highly volatile hydrophobic small molecules responsible for their aroma, taste, and pungency. Empirically, we understand that these compounds can evoke a sweet taste; however, their specific interactions with sweet taste receptors are unclear. To address this issue, HEK293 cells expressing human and mouse sweet taste receptors TAS1R2/TAS1R3 were used to identify *trans*-2-hexenal (a novel sweetener) in human and cinnamyl alcohol (a sweetness inhibitor) in mice. The effects of these compounds on TAS1R2/TAS1R3 in humans and mice were evaluated alongside known hydrophobic sweet compounds, and the results showed that they elicited responses in human TAS1R2/TAS1R3 but not in mice. Conversely, some compounds inhibited the sweetness of sucralose both in vitro and in vivo. Response analysis using human and mouse chimeric TAS1R2 and point mutants of TAS1R2 using docking simulations indicated that these compounds bind to the transmembrane domain of TAS1R2 and that multiple amino acid residues are essential to generate a sweet taste. These results indicate that highly volatile hydrophobic compounds generate aroma and sweetness through a different mechanism than hydrophilic sweeteners, such as sucrose.

Keywords Sweet taste, Aroma compound, GPCR, Species difference

Plants contain a variety of low-molecular-weight (MW) compounds, and when consumed, these compounds convey tastes, aromas, and somatic sensations such as pungency. Some hydrophilic compounds in plants are believed to impart a pleasant taste. Typical examples are monosaccharides and disaccharides such as glucose, fructose, and sucrose, which convey sweet tastes¹, because they bind to the sweet taste receptor TAS1R2/TAS1R3². Glutamate is an amino acid that produces a savory sensation referred to as *umami*¹ by binding to the amino acid (umami) taste receptor TAS1R1/TAS1R3³. TAS1R1, TAS1R2, and TAS1R3 form the TAS1R family and are classified as class C G protein-coupled receptors (GPCRs), which possess three domains: the ligand-binding domain (LBD), cysteine-rich domain (CRD), and transmembrane domain (TMD)⁴. Most hydrophilic sweet compounds bind to the LBDs of TAS1R2 and TAS1R3; a few sweet compounds, such as the artificial sweetener cyclamate⁵ and sweet inhibitors such as lactisole⁶ and gymnemic acid, bind to the TMD of TAS1R3⁷, and umami compounds such as glutamic acid and nucleic acid, bind to the LBD of TAS1R1⁸.

Plants contain a wide variety of hydrophobic compounds, many of which are bitter, such as quinine (logP = 2.9, MW 324.4), an alkaloid found in the bark of the cinchona tree, and quercetin (logP = 1.5, MW 302.23), a typical dietary flavonoid. Some studies have suggested a correlation between hydrophobicity and bitterness⁹. Bitter substances bind to the TAS2R family, which are class T GPCRs that have no extracellular domain, similar to odorant receptors¹⁰. However, not all bitter substances are highly hydrophobic, such as caffeine (logP = −0.1, MW 194.19) and many plant polyphenols. Furthermore, some reports have indicated that hydrophobicity is not an indicator of bitterness^{11,12}. Many hydrophobic compounds in plants have low MWs (generally < 300) and can be volatilized to produce aromas, such as limonene (logP = 3.4, MW 136.23), the aroma of lemon, and 2,6-nonadien-1-ol (logP = 2.1, MW 140.22), the aroma of cucumber.

¹Institute of Food Research, National Agriculture and Food Research Organization (NARO), 2-1-12 Kannondai, Tsukuba 305-8642, Japan. ²Section of Oral Neuroscience, Graduate School of Dental Science, Kyushu University, Fukuoka, Japan. ³Oral Health/Brain Health/Total Health Research Center, Graduate School of Dental Science, Kyushu University, Fukuoka, Japan. ⁴Research and Development Center for Five-Sense Devices, Kyushu University, Fukuoka, Japan. ⁵Tokyo Dental Junior College, Tokyo, Japan. ⁶Monell Chemical Senses Center, Philadelphia, PA, USA. ⁷Division of Biomedical Science, Faculty of Medicine, University of Tsukuba, Tsukuba, Japan. ⁸Transborder Medical Research Center, University of Tsukuba, Tsukuba, Japan. ⁹Graduate School of Medicine, Dentistry and Pharmaceutical Sciences, Okayama University, Okayama, Japan. ¹⁰Present address: Institute for Protein Research, Osaka University, Suita, Japan. ✉email: ykusa@affrc.go.jp

Plants also contain hydrophobic, low-MW, sweet compounds. The following compounds are known only empirically: anethole¹³, the main aromatic component of fennel (*Foeniculum vulgare*); cinnamaldehyde¹⁴, the main aromatic component of cinnamon (*Cinnamomum verum*); and perillartine, a non-aromatic component of shiso herbs (*Perilla frutescens* var. *crispa*) that acts on TAS1R2-TMD (Table 1, Table S1, Fig. S1)¹⁵. However, the effects of hydrophobic sweet compounds other than perillartine on TAS1R2/TAS1R3 and their sensory characteristics have not been widely investigated. Although no low-MW hydrophobic compound with an umami flavor has been identified, methional (logP = 0.3, MW = 104.17), a notable flavor in potato chips, cheese, and soy sauce, is known to enhance the umami taste¹⁶. Unlike glutamate, methional binds to human TAS1R1-TMD and acts as a positive allosteric modulator (PAM), which enhances umami; however, when methional binds to mouse TAS1R1-TMD, it elicits a negative allosteric modulator (NAM) effect, which suppresses the umami taste.

With reference to this methional property, we predicted that low-MW sweet compounds would have different binding properties from hydrophilic sweet compounds. To investigate this, we identified novel hydrophobic sweet compounds and investigated their binding affinity to TAS1R2/TAS1R3.

Results

Novel sweet plant aroma compounds

Two approaches were used to identify novel hydrophobic sweet compounds. Anethole and cinnamaldehyde are phenylpropenes widely recognized as key aromatic components of many spices and herbs¹⁷. Thus, we first focused on analogs of anethole and cinnamaldehyde and examined the responses of the human sweet taste receptor TAS1R2/TAS1R3 in HEK293 cells to cinnamyl alcohol, methyl cinnamate, cinnamate, and vanillin. We then focused on cinnamaldehyde and perillaldehyde, which are agonists of the pungency receptor TRPA1 and analogs of perillartine, which is found in many spices¹⁸. Although many plant components are TRPA1 agonists¹⁹, we focused on *trans*-2-hexenal²⁰, a sweet aroma compound found in apples and other fruits. Human TAS1R2/TAS1R3 responses were analyzed for *trans*-2-hexenal and the known hydrophobic sweet compounds anethole, cinnamaldehyde, and perillartine. Significant responses to human TAS1R2/TAS1R3 were observed for *trans*-2-hexenal, anethole, perillartine, and cinnamaldehyde (Fig. 1A). In contrast, no response was observed when these compounds were applied to mouse TAS1R2/TAS1R3 (Fig. 1B). A previous report found that methional, a hydrophobic food ingredient, inhibits responses at the mouse umami receptor TAS1R1/TAS1R3¹⁶. Consequently, the effects of sucralose (1 mM) on TAS1R2/TAS1R3 were also investigated. The addition of perillartine, cinnamaldehyde, or cinnamyl alcohol inhibited the response to sucralose (1 mM) in mice TAS1R2/TAS1R3 (Fig. 1C). We examined whether the results obtained from the in vitro experiments also occurred in vivo. The sweetness intensity of water, *trans*-2-hexenal (5 mM), and sucrose (50 mM) in the oral cavity were evaluated and compared among 11 participants using visual analog scale (VAS) scores. All methods were conducted in accordance with the Declaration of Helsinki, and all participants provided written informed consent to participate in the study. As *trans*-2-hexenal has a leafy-green, sweet bluish aroma, a nose clip was used to remove the influence of the aroma on taste perception. Sweetness intensity differed significantly among the solutions ($F_{(2,20)} = 23.3$, $p < 0.001$, effect size (f) = 1.53). The sweetness intensity of *trans*-2-hexenal (5 mM) was greater than that of water ($p < 0.001$, effect size (d) = 1.71). There was no significant difference in sweetness intensity between *trans*-2-hexenal (5 mM) and sucrose (50 mM; $p = 0.45$, effect size (d) = 0.24; Fig. 2). Cinnamyl alcohol and perillartine were found to significantly inhibit the sweet taste in mouse TAS1R2/TAS1R3 response measurements. Consequently, taste nerve response measurements were obtained to eliminate the effects of aroma and other sensory effects. All animal experiments were conducted in accordance with the ARRIVE and AVMA guidelines.

There was no nerve response observed for cinnamyl alcohol and perillartine alone according to the criteria that voltages during stimulation were larger than the mean plus 2 SDs of the voltages for 10 s periods before and after stimulation. Then we measured the effect of cinnamyl alcohol and perillartine on taste responses using the entire nerve. We applied these hydrophobic compounds to bind TAS1R2/TAS1R3 before application of taste solutions. Sample recordings of the integrated whole-nerve responses from the chorda tympani (CT) nerves of C57BL/6J mice are shown in Fig. 3A. The application of cinnamyl alcohol (1.5 mM) affected the response to

Compound	LogP	MW	Solubility (water; mg/mL)	Vapor pressure (mmHg)	Scent
sucralose	−1.5	397.6	22.7	4.0×10^{-14}	n. d.
<i>trans</i> -2-hexenal	1.5	98.1	insoluble	6.6	green
anethole	3.3	148.2	insoluble	5.0×10^{-2}	licorice
perillartine	2.9	165.2	insoluble	8.5×10^{-5}	n. d.
cinnamaldehyde	1.9	132.2	1.4	2.9×10^{-2}	spicy
cinnamyl alcohol	1.5	134.2	1.8	1.2×10^{-2}	balsamic
methyl cinnamate	2.6	176.2	insoluble	5.5×10^{-3}	balsamic
ethyl cinnamate	3	176.2	insoluble	4.5×10^{-2}	balsamic
cinnamic acid	2.1	148.2	0.5	5.0×10^{-3}	balsamic
vanillin	1.2	152.2	10.0	1.2×10^{-4}	vanilla

Table 1. Chemical properties of the compounds used in this study. Compound properties were obtained from PubChem and chemical vendors. n.d.: not determined. MW: molecular weight.

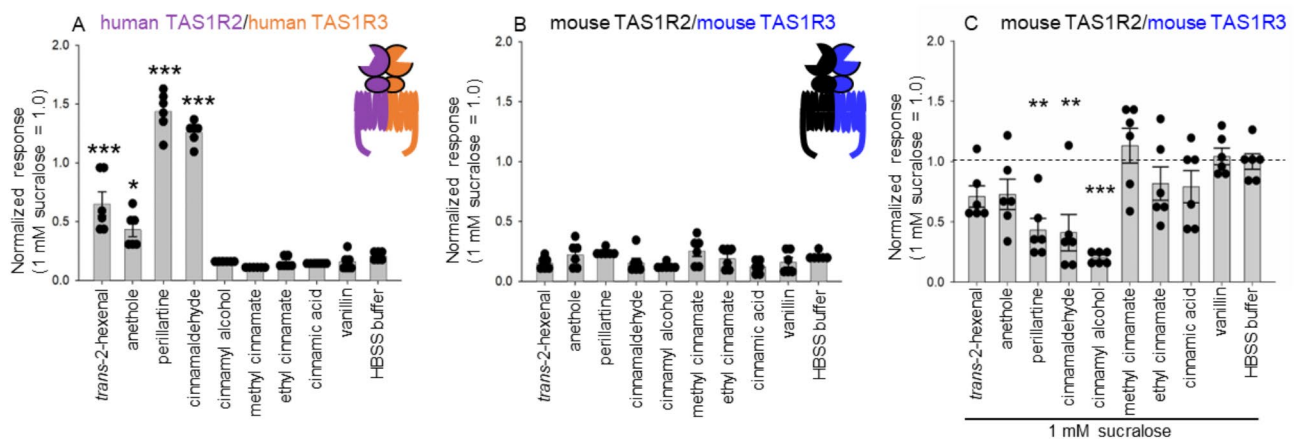


Fig. 1. Response, enhancement, and inhibition of human and mouse TAS1R2/TAS1R3 by hydrophobic compounds. Ca^{2+} influx into HEK293 cells expressing human TAS1R2/TAS1R3 (A) and mouse TAS1R2/TAS1R3 (B, C) was monitored using the Fluo8 NW indicator. For each compound, 5 mM of the solution was applied to the cells, unless there was a nonspecific response. Perillartine and cinnamaldehyde were applied at 0.2 and 1 mM, respectively, without a nonspecific response. The responses of hydrophobic compounds to human and mouse TAS1R2/TAS1R3 are shown in (A) and (B), respectively. The responses of human and mouse TAS1R2/TAS1R3 cells to hydrophobic compounds mixed with sucralose (1 mM) are shown in (C). The statistical significance between the responses to compounds and the control, Hanks' balanced salt solution (HBSS), for A, B, and sucralose (1mM; no ligand) for C, were evaluated using the Dunnett method. *, **, and *** indicate $p < 0.05$, $p < 0.01$, and $p < 0.001$ vs. the control (HBSS buffer or sucralose [1mM]), respectively. Error bars indicate standard error (SE; $n = 6$).

sucralose among stimuli containing 5 primary taste compounds. The effects of a 0.25–1.5 mM concentration series of cinnamyl alcohol or perillartine on sucralose (10 mM) were examined (Fig. 3B). The response to 10 mM sucralose was significantly suppressed by cinnamyl alcohol (one-way ANOVA, effect of the hydrophobic compounds: $F_{(3, 20)} = 4.679$, $p = 0.012$) and perillartine ($F_{(3, 16)} = 3.949$, $p = 0.028$) in a dose-dependent manner. After gurmarin treatment, suppression by these hydrophobic compounds was not detected ($p = 0.748$ for cinnamyl alcohol and $p = 0.147$ for perillartine). Furthermore, the inhibitory effect of gurmarin was evident in the responses to 10 mM sucralose with or without 0.25–1.5 mM of the hydrophobic compounds (repeated measures ANOVA, effect of gurmarin: $F_{(1, 27)} = 53.44$, $p < 0.001$ for sucralose + cinnamyl alcohol, $F_{(1, 24)} = 83.75$, $p < 0.001$ for sucralose + perillartine). These results indicate that the response to sucralose and its inhibition by hydrophobic compounds occurs through TAS1Rs.

Functional domains of hydrophobic sweeteners/inhibitors in TAS1R2

It was speculated that hydrophobic sweet compounds are likely to bind to TAS1R2-TMD because hydrophobic compounds, such as perillartine, S819, and P4000, bind TAS1R2-TMD (Table S1, S2) and methional acts on TAS1R1-TMD¹⁶. Therefore, we created chimeric mutants in which TAS1R2-TMD was exchanged between human and mouse TAS1R2/TAS1R3 cells and observed the enhancement/inhibition of their responses using cinnamaldehyde, cinnamyl alcohol, and perillartine (Fig. 4). For mutant analysis, we transiently expressed each mutant receptor in HEK293 cells and applied repeated stimulation using a perfusion system (transient multiple stimulation system; Fig. 4). While the stable cell line (stable single stimulation system; Fig. 1) is effective for screening sweet compounds, it is less suitable for comparing responsiveness between mutants because of potential biases in gene copy number. Therefore, we used a transient multiple-stimulation approach that allowed for appropriate response comparisons via perfusion. Given the variability in n (sample size), responses or inhibition were only considered to have been observed when there was both a significant difference ($p < 0.05$) and an effect size (Cohen's d) of < 0.8 . When the TAS1R2-TMD of human TAS1R2/TAS1R3 was replaced with the mouse-derived equivalent (chimera Hm2/H3), none of the compounds elicited responses while maintaining the responses of sucralose, which binds to TAS1R2-LBD, and cyclamate, which binds to human TAS1R3-TMD (Fig. 4B). In contrast, when the TAS1R2-TMD of mouse TAS1R2/TAS1R3 was replaced with the human-derived equivalent (chimera mH2/m3), cinnamaldehyde and perillartine responses were observed (Fig. 4C). To examine the ability of the chimeric mutants to enhance or inhibit sweetness, they were stimulated with sucralose (1 mM) and a mixture of cinnamaldehyde, cinnamyl alcohol, or perillartine. When the TAS1R2-TMD of human TAS1R2/TAS1R3 was replaced with the mouse-derived equivalent (chimera Hm2/H3), sweetness was inhibited by the addition of cinnamyl alcohol (Fig. 4F). When the TAS1R2-TMD of mouse TAS1R2/TAS1R3 was replaced with the human-derived equivalent (chimera mH2/m3), the inhibitory effect of sweetness on cinnamyl alcohol observed in mouse TAS1R2/TAS1R3 (Fig. 4H) disappeared (Fig. 4G). Although there were some differences in the results compared with those obtained with HEK293 cells stably expressing these mutants, both sets of results indicated that the presence of human TAS1R2-TMD caused a sweet taste response to hydrophobic sweet compounds, whereas the presence of mouse TAS1R2-TMD inhibited this sweet taste response (Fig. S2).

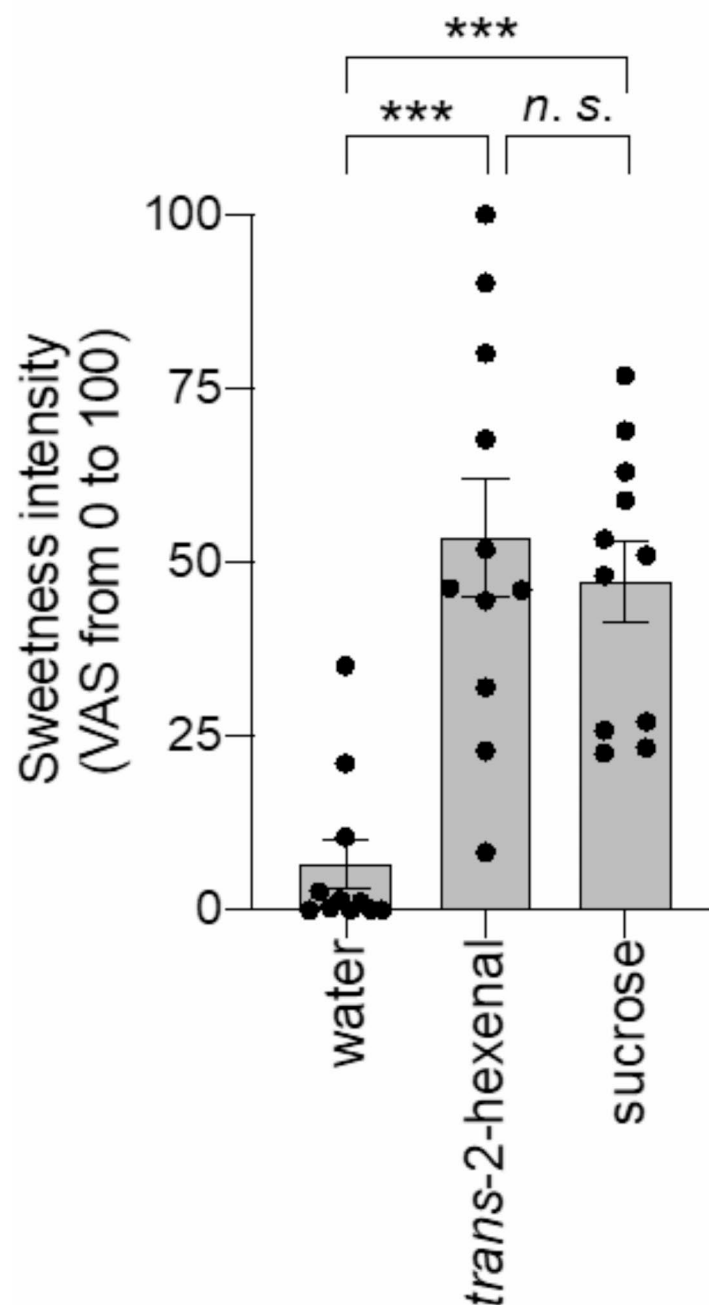


Fig. 2. Verification of *trans*-2-hexenal sweetness by sensory evaluation. The sweetness intensities of *trans*-2-hexenal (5 mM) and sucrose (50 mM) were rated using a visual analog scale (VAS). Water was used as a negative control. Statistical significance among the solutions was evaluated using repeated measures one-way ANOVA, followed by the Holm–Sidak test. *** $p < 0.001$. Error bars indicate standard error (SE; $n = 11$; six males and five females, 23–49 years old).

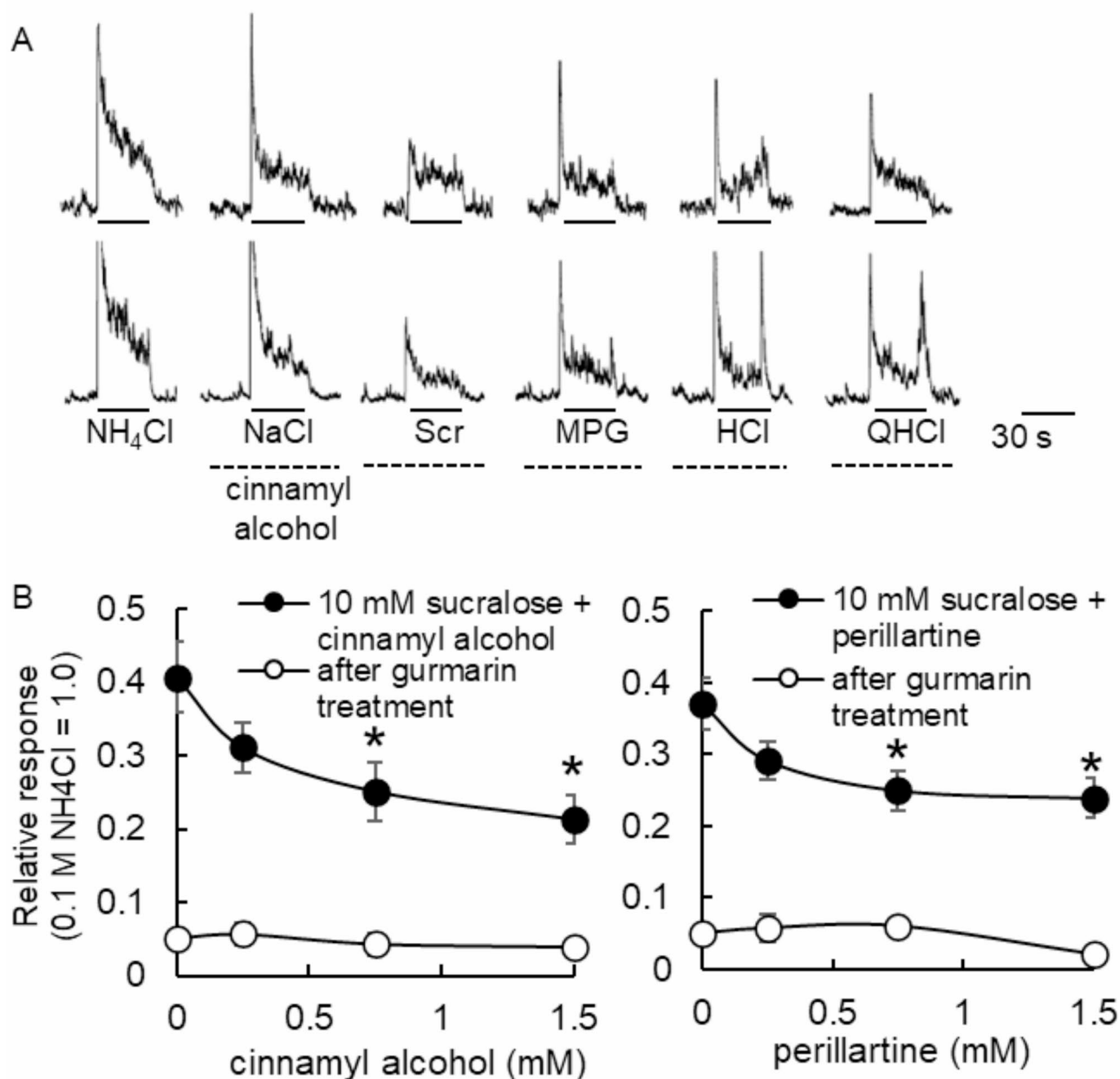


Fig. 3. Verification of cinnamyl alcohol and perillartine sweetness inhibition using electrophysiological analysis in mice. (A) Sample recordings of integrated whole-nerve responses from the chorda tympani nerve of C57BL/6J mice. The stimuli were NH_4Cl (100 mM; standard stimulus), NaCl (100 mM), sucralose (10 mM; Scr), monopotassium glutamate (300 mM; MPG), HCl (10 mM), and quinine HCl (20 mM; QHCl). The bars indicate the application of stimuli. In lower recordings, these non-standard stimuli were mixed with 1.5 mM cinnamyl alcohol, and the cinnamyl alcohol solutions were applied to the tongue before and after the application mixtures. (B) Effects of cinnamyl alcohol and perillartine on whole-nerve responses to 10 mM sucralose before (closed circles) and after (open circles) application of gurmarin to the tongue ($n=5-6$). Values are means \pm SE. Post hoc Dunnett's method; * $p < 0.05$.

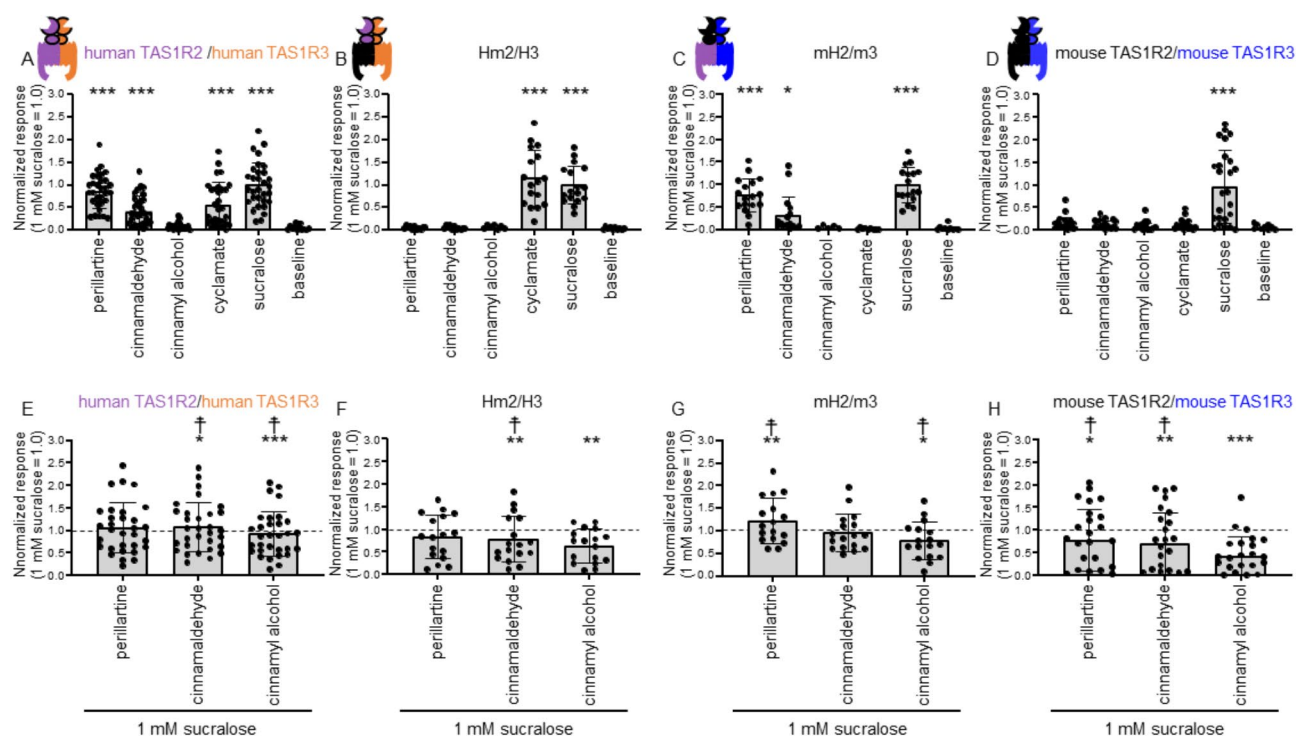


Fig. 4. Responses of chimeric mutants to hydrophobic compounds. Responses to hydrophobic compounds were measured in HEK293 cells transiently expressing human TAS1R2/TAS1R3 chimeric receptor with the transmembrane region of TAS1R2 replaced with mouse (Hm2/H3), mouse TAS1R2/TAS1R3 chimeric receptor with the transmembrane region of TAS1R2 replaced with human (mH2/m3), and mouse TAS1R2/TAS1R3. Sucralose (1 mM), perillartine (0.2 mM), cinnamaldehyde (0.3 mM), cinnamyl alcohol (1 mM), and cyclamate (30 mM) were used. The upper column shows the response produced by the hydrophobic compounds, and the lower column shows the effect of adding hydrophobic compounds on the sweetness response to sucralose (1 mM). Data are expressed as the mean \pm SD of 15–31 cells ($n = 3$). *, **, and *** indicate $p < 0.05$, $p < 0.01$, and $p < 0.001$, respectively, vs. the control (baseline or 1 mM sucralose), as determined using repeated measures one-way ANOVA and Tukey's post-hoc test. † an effect size (Cohen's d) < 0.8 , indicating a statistically significant but not practically meaningful difference.

Docking simulations using the proposed human TAS1R2-TMD model obtained from AlphaFold 2 were performed to clarify the agonistic mechanism of hydrophobic molecules in human TAS1R2-TMD and antagonist mechanism in mouse TAS1R2-TMD. Perillartine was used in the docking simulations because of the tested compounds and was expected to exhibit the most stable binding to TAS1R2-TMD (Fig. 4). Docking simulations between perillartine and TAS1R2-TMD were performed using the TAS1R2-TMD/TAS1R3-TMD heterodimer model (see Methods for details). The predicted binding sites for perillartine differed between humans and mice, whereas most predicted binding sites had the same amino acid sequences in humans and mice (Fig. 5). Among the residues predicted to be binding sites in human TAS1R2, residue Y769 in the sixth transmembrane domain (TM6) differed from that in mouse TAS1R2. Residue Y769 corresponds to human TAS1R1-N761, which contributes significantly to the ability of methionine to enhance umami in human TAS1R1/TAS1R3 and suppress umami in mouse TAS1R1/TAS1R3¹⁶. Thus, it was predicted that human TAS1R2-Y769 would also contribute significantly to the phenomenon of perillartine becoming an agonist in humans and an antagonist in mice, and consequently, a mutant that replaced human TAS1R2-Y769 and mouse TAS1R2-S773 was created (Fig. 5). We also created mutants substituted for alanine in human TAS1R2-L728, mouse TAS1R2-L732, human TAS1R2-T736, and mouse TAS1R2-L732, which are the residues in the fifth transmembrane domain (TM5) of human TAS1R2-TMD or mouse TAS1R2-TMD that are predicted to be the most likely to bind perillartine (Fig. 5).

The responses of the mutants were observed with point mutations introduced into the TAS1R2-TMD to hydrophobic sweet compounds, specifically cinnamaldehyde, cinnamyl alcohol, and perillartine, based on the results in Fig. 1 (Fig. 6). Interestingly, human TAS1R2-Y769S (hTAS1R2Y769S) abolished the response to cinnamaldehyde and perillartine (Fig. 6B), whereas responsiveness to sucralose and cyclamate remained. Human TAS1R2-L728A (hTAS1R2L728A) showed a significant response to cinnamaldehyde and perillartine (Fig. 6C). Human TAS1R2-T732A (hTAS1R2T732A) responded to cinnamaldehyde and perillartine (Fig. 6D) and suppressed the sweetness of cinnamyl alcohol (Fig. 6H). Point mutations in mouse TAS1R2 (mTAS1R2S773Y

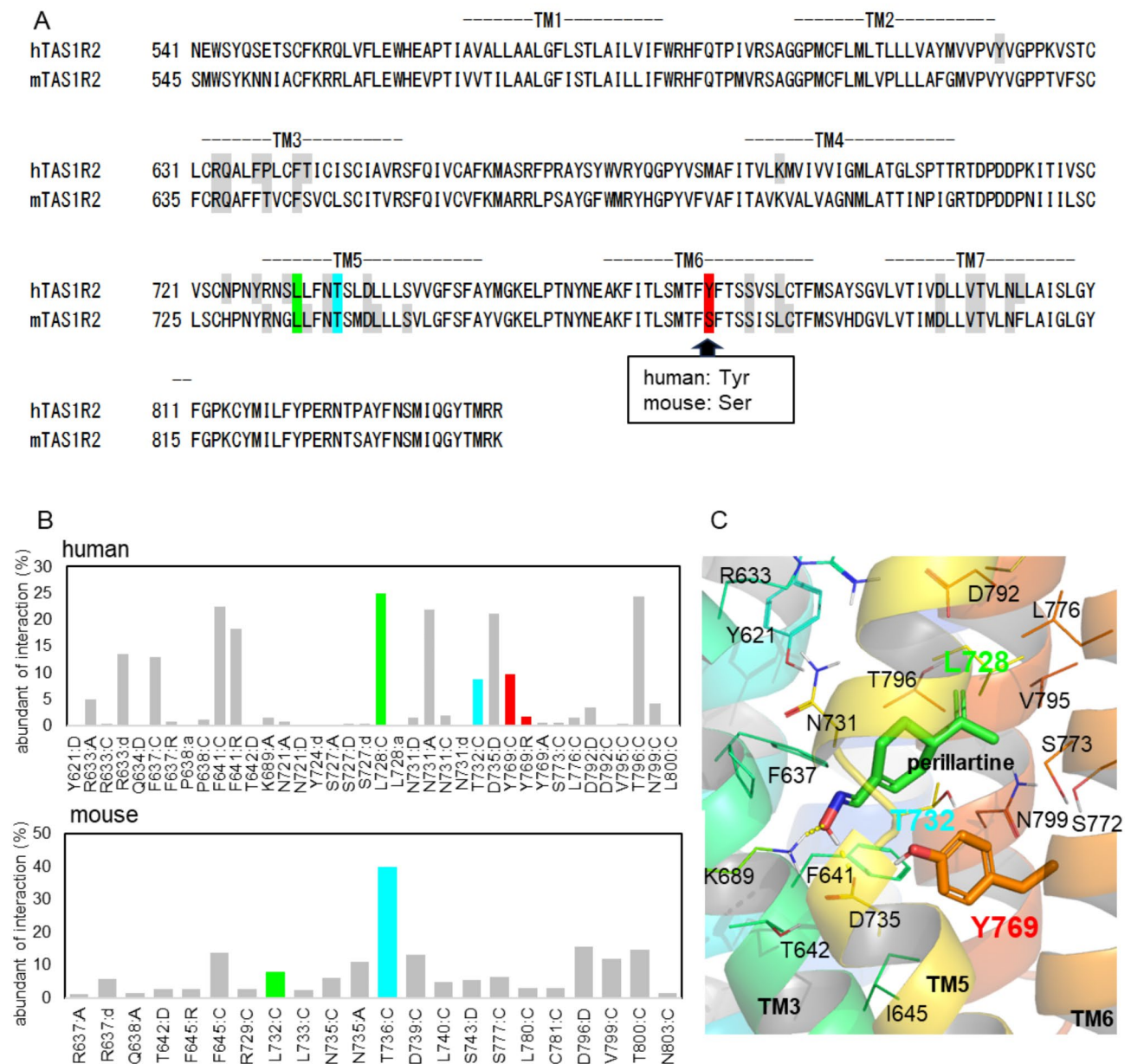


Fig. 5. Interaction analysis of perillartine binding with TAS1R2-TMD using an MD simulation. (A) Alignments of human TAS1R2 (hTAS1R2) and mouse TAS1R2 (mTAS1R2) transmembrane domains. The gray, green, blue, and red backgrounds indicate the residues used for the population diagrams in B, and the green, blue, and red backgrounds indicate the residues for the point mutants of hTAS1R2L728A, hTAS1R2T732A, mTAS1R2T736A, hTAS1R2Y769S, and mTAS1R2S773Y in Fig. 6. (B) Population diagram showing the amino acid interactions between perillartine and TAS1R2 (top: human and bottom: mouse) during the MD simulation represented in a fingerprint scheme by the protein-ligand interaction fingerprint analysis. The interaction fingerprint was used to evaluate hydrogen-bonding, ionic attraction, arene attraction, and surface contact. X-axis labels are represented by residue information and interaction type across the colon. Interaction type is expressed in the following abbreviations: sidechain hydrogen bond donor [D], sidechain hydrogen bond acceptor [A], backbone hydrogen bond donor [d], backbone hydrogen bond acceptor [a], arene attraction [R] and total surface contact [C]. (C) Snapshot structure showing the state most in contact with the Tyr769 residue in the MD calculations for the perillartine and human TAS1R2 complex.

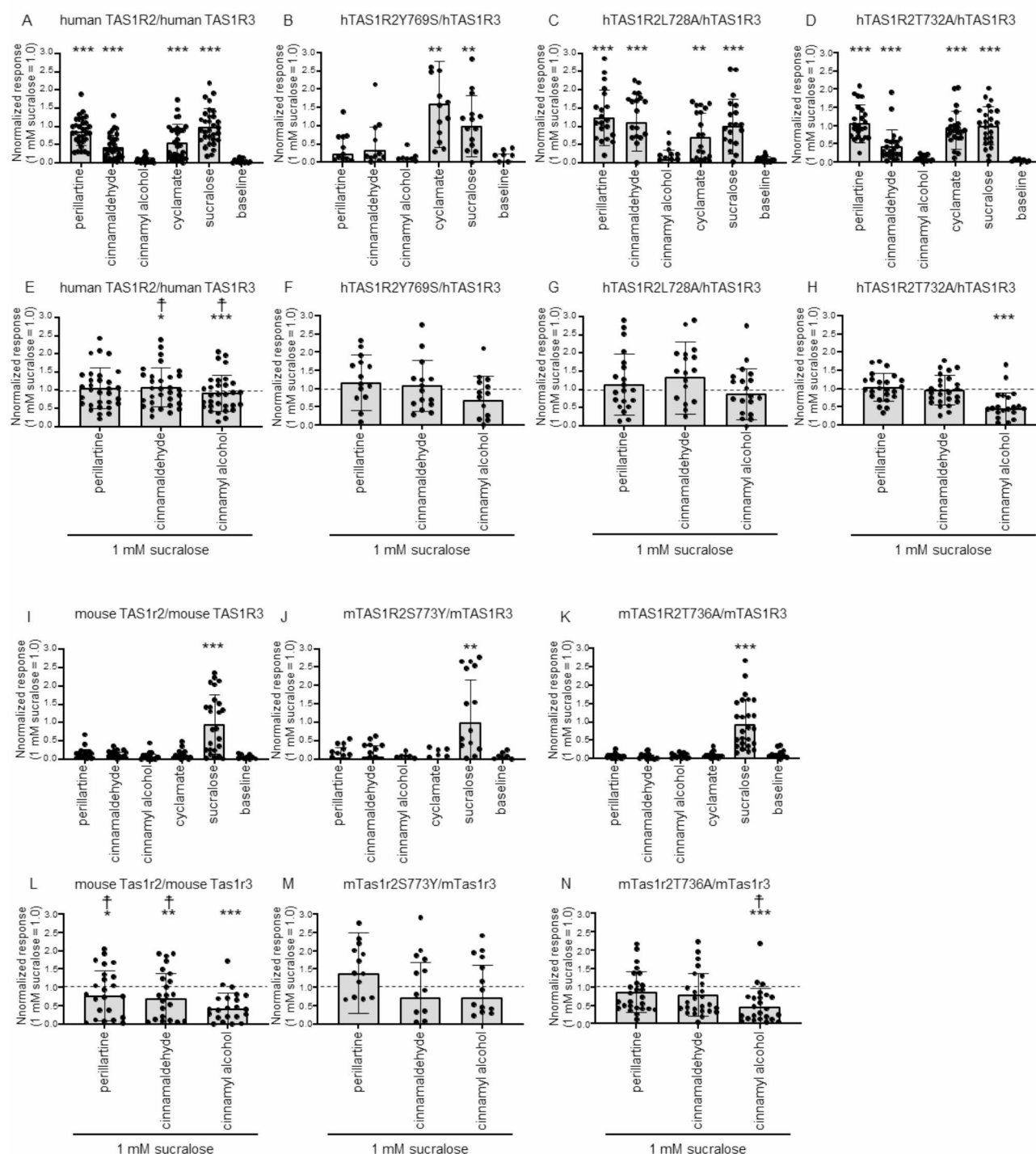


Fig. 6. Responses of human and mouse TAS1R2-TMD point mutants to hydrophobic compounds. Responses to hydrophobic compounds were measured in HEK293 cells transiently expressing full-length human or point mutants of TAS1R2 and TAS1R3. Sucralose (1 mM), perillartine (0.2 mM), cinnamaldehyde (0.3 mM), cinnamyl alcohol (1 mM), and cyclamate (30 mM) were used. The vertical axis represents the response intensity relative to that of sucralose (1 mM). A–D and I–K show the responses produced by hydrophobic compounds, and E–H and L–N show the effects of adding hydrophobic compounds on the sweetness response to sucralose (1 mM). Data are expressed as the mean \pm SD of 15–31 cells ($n=3$). *, **, and *** indicate $p < 0.05$, $p < 0.01$, and $p < 0.001$, respectively, vs. the control (baseline or sucralose [1 mM]), determined using repeated measures one-way ANOVA and Tukey's post-hoc test. † an effect size (Cohen's d) < 0.8 , indicating a statistically significant but not practically meaningful difference. To provide a basis for comparison, A, E, I, and L reference the data from Fig. 4 A, E, D, and H.

				TM6
human	TAS1R2	761	FITLSMTFY	FTSSVSLCTFMS
mouse	TAS1R2	765	FITLSMTFS	FTSSI SLCTFMS
squirrel	TAS1R2	765	FITLSMTFS	FTSSVSLCTFMS
rabbit	TAS1R2	754	FITLSMTFS	FTSTVSLCTFMS
cattle	TAS1R2	759	FITFCMTFY	FSSSVFLCTFMA
Tasmanian devil	TAS1R2	759	FITLSVTFY	FVSSVFLCTFVS
platypus	TAS1R2	759	FITLNMTFY	FTSSVSLCTFMS

Fig. 7. Comparison of human TAS1R2-Y769 residues in various species. The amino acid sequences of the sixth transmembrane region of TAS1R2-TMD, including human TAS1R2-Y769, were compared. Human, mouse, squirrel, rabbit, cattle, Tasmanian devil, and platypus were selected as representative mammalian species and for rodent comparison. The gene IDs (NCBI ID) were as follows: human, NM_152232.4; mouse, NM_031873.1; rabbit, XP_051714014.1; squirrel, XP_026256637.1; cattle, NM_001206529.3; Tasmanian devil, XP_031818607; and platypus, XP_02891786.

and mTAS1R2T736A) resulted in a response similar to that of wild-type mouse TAS1R2 (Fig. 6J, K). The mTAS1R2S773Y and mTAS1R2T736A mutants abolished cinnamyl alcohol-induced inhibition (Fig. 6M, N).

Responses to sweet compounds in HEK293 cells expressing mTAS1R2L732A were not observed using Ca^{2+} imaging (Fig. S3). The responses of hTAS1R2Y769S and mTAS1R2S773Y to sucralose were weaker than those of wild-type hTAS1R2 and mTAS1R2 (Fig. S3).

The sweetness of some sweeteners, including artificial sweeteners, was thought to have been acquired during evolution^{21–23}. Therefore, to assess whether the acquisition of sweet taste mechanisms in TAS1R2-TMD occurred during mammalian evolution, we searched the database for species-specific differences in the human TAS1R2-Y769 residues. (Fig. 7). To elucidate the broader implications of mammalian evolution, we examined the human TAS1R2-Y769 in diverse species representing different orders and evolutionary lineages. Residues corresponding to human TAS1R2-Y769 were analyzed in *monotremes* (platypus), *marsupials* (Tasmanian devil), and *placentals* (cattle) belonging to *Laurasiatheria*, which are evolutionarily distinct from humans and mice. The results revealed a consistent tyrosine residue at this position across all species, which is similar to the human sequence. Further exploration involved species from the orders *Rodentia* (squirrels) and *Rabbitiformes* (rabbits), and the residue corresponding to mice showed a shared evolutionary pattern within these orders.

Discussion

This study identified novel volatile hydrophobic sweet compounds from plant aroma substances and demonstrated that *trans*-2-hexenal can be used as a novel sweetener. Novel and well-known hydrophobic sweet compounds were also found to act as sweetness inhibitors in mice. We demonstrated that hydrophobic sweet compounds bind to TAS1R2-TMD, whereas many hydrophilic sweet compounds bind to TAS1R2-LBD. The identified interactions between food components and TAS1R2/TAS1R3 will ultimately help clarify the nature of sweetness.

Sweet-taste receptors bind sweet compounds at various sites (Fig. S4). In human TAS1R2/TAS1R3, most sweet compounds bind to TAS1R2-LBD, whereas some sweet and inhibitory compounds bind to TAS1R3-TMD⁷. Our results showed that cinnamaldehyde and cinnamyl alcohol act on TAS1R2-TMD, which has previously been shown to bind the natural sweetening compound perillartine¹⁵, the non-natural sweet compounds S819⁸ and P4000²⁴, and the inhibitory compound amiloride²⁵. The fact that a single receptor accepts multiple ligands with multiple binding domains indicates that each domain accepts a substantial number of sweet compounds with a rule-based role assignment. Here, we discuss the physical properties and chemical structures of the compounds that bind to TAS1R2-TMD.

Sweet compounds that bind to TAS1R2-TMD share several common physical properties: they have logP values ranging from 1 to 3.3, low solubility, and low molecular weights (Table 1, Table S1, S2). However, the volatility varies widely, there is no clear correlation between aromaticity and sweetness. In contrast, compounds that bind to TAS1R2-LBD cover a broader range of molecular sizes, from small molecules like glucose (MW 180) to large molecules like miraculin (24.6 kDa). This indicates that a low MW alone may be insufficient for TAS1R2-TMD binding. In addition, natural products binding to TAS1R2-LBD are hydrophilic and water-soluble, such as glucose and sucrose, which distinguishes them from compounds binding to TAS1R2-TMD. In contrast, compounds that bind to TAS1R3-TMD, such as lactisole and gymnemic acid, exhibit differences in solubility

and logP values, indicating that they have different binding modes from TAS1R2-TMD. Compounds binding to TAS1R1-TMD, such as methional (MW 104, logP = 0.3, solubility = 163 mg/mL), also differ from those binding to TAS1R2-TMD in terms of solubility and MW, indicating that binding mechanisms vary. There was no common chemical structure among the compounds that bound to TAS1R2-TMD. This structural diversity suggests that the binding mode is not uniform. However, there are several shared common structures. Cinnamaldehyde, anethole, cinnamyl alcohol, cinnamic acid, methyl cinnamate, and ethyl cinnamate are phenylpropenes (Fig. S1). They were divided into those that acted as ligands for TAS1R2/TAS1R3 and those that did not. Anethole and vanillin, along with the artificial sweeteners P4000 and S819 (Table S2, Fig. S5), all possess a phenylether structure; however, only vanillin did not activate human TAS1R2/TAS1R3. Thus, these common structures are unlikely to be related to human TAS1R2/TAS1R3 activation.

It is possible that hydrophobic sweet compounds bind outside of TAS1R2-TMD. The chimera mH2m3 exhibited a smaller sweetness response than the chimera H2m3 (Fig. 5), and compounds with significant responses were limited to perillartine and cinnamaldehyde. Thus, the possibility that sweet hydrophobic compounds act as adjuncts to TAS1R2-LBD and TAS1R2-CRD cannot be ruled out. It is possible that hydrophobic sweet compounds may also act as adjuncts to TAS1R3, as the response appears to be greater with chimera Hm2H3 than chimera Hm2m3, although the difference was not significant (Fig. S2). The nature of the stable cells used in this study may have affected the results; consequently, further research will be required in the future.

This study has also shown that several natural hydrophobic compounds that bind to human TAS1R2-TMD and produce a sweet taste function act as sweet taste inhibitors with mouse TAS1R2-TMD. Gurmarin and amiloride are sweetness inhibitors in mice. Specifically, gurmarin is a 35-residue polypeptide that was isolated from the leaves of *Gymnema Sylvestre*²⁶ and acts on TAS1R2 and TAS1R3 in the LBD (unpublished data). In contrast, amiloride is a diuretic and known inhibitor of epithelial-type sodium ion channels²⁷ and has also been shown to act on TAS1R2-TMD to inhibit sweet tastes in both humans and mice, but not in squirrel monkeys²⁵. Furthermore, perillartine binds to TAS1R2-TMD in humans and induces sweetness¹⁵ but has not previously been shown to inhibit sweetness in mice. This is the first time that multiple natural sweetness inhibitors have been found to bind to the same domain of mouse TAS1R2/TAS1R3, increasing the possibility that mouse TAS1R2-TMD is the major inhibitory domain for sweet taste reception. However, we are skeptical that sweet taste inhibition via TAS1R2-TMD has a critical effect on the mouse food environment. This is because sweet taste response inhibition by cinnamyl alcohol and perillartine was more limited than that by gurmarin, as shown in the neural response measurement results for mice (Fig. 3). Without further insight into whether a stronger inhibitor exists, it is premature to draw definitive conclusions.

The results show that the binding sites for sweetness inhibitors differ between humans and mice, indicating that structure and function may be fundamentally different between human TAS1R2/TAS1R3 and mouse TAS1R2/TAS1R3 (Fig. S4). In human TAS1R2/TAS1R3, many sweet compounds bind to TAS1R2-LBD^{8,28,29} and TAS1R3-TMD^{5,30}, and many sweet inhibitors bind to TAS1R3-TMD^{6,31}, that is, agonists and antagonists bind to different molecules. In contrast, this study revealed that mouse TAS1R2/TAS1R3 antagonists bind to TAS1R2-TMD, suggesting that agonists and antagonists bind to the same molecule at different sites to modulate the sweet taste. Because mouse TAS1R1 also binds amino acids to TAS1R1-LBD³ and the antagonist methional to TAS1R1-TMD¹⁶, it may have a similar structural function in TAS1Rs. However, TAS1R1-TMD and TAS1R2-TMD do not act in the same way; methional bound to TAS1R1-TMD acts as a PAM in humans and as a NAM in mice, and residues such as TAS1R1-N761 are involved in the PAM/NAM switching process. In this study, docking simulations showed that perillartine binds to TAS1R2-Y769, which corresponds to TAS1R1-N761. However, the TAS1R2-Y769 mutation did not switch the human TAS1R2 response from sweetness to the inhibitory response observed in mice. In addition, W648, which is highly conserved in the TM6 of class C GPCRs and is known to play an important role in the toggle-switch mechanism that triggers conformational changes associated with receptor activation³², is not conserved in TAS1R2 (S773 in human TAS1R2 and S777 in mouse TAS1R2). Therefore, it is necessary to carefully consider whether hydrophobic compounds bound to TAS1R2-TMD act as PAMs and whether TAS1R2-Y769 is involved in the PAM/NAM switch mechanism. The structural function of a receptor is not only to accept compounds but also to translocate them to the plasma membrane and stabilize their structures³³. The point mutations hTAS1R2-Y769 and mTAS1R2-L732A reduced sucralose binding to TAS1R2-LBD, suggesting that these mutations affect the overall structural function of TAS1R2/TAS1R3. Future structure-function analyses based on these findings are required.

The evolutionary aspects of species differences in human TAS1R2 Y769 and mouse TAS1R2 S773, which are critical sites for the binding of hydrophobic sweet compounds to TAS1R2, were investigated. The sweetness of the artificial sweetener cyclamate and the inhibition of sweetness by gymnemic acid in the leaves of *Gymnema sylvestre* may have acquired their effects on TAS1R3-TMD during primate evolution^{22,23}. Species-specific comparisons of the residues in human TAS1R2-TMD Y769 did not indicate that TAS1R2-TMD acquired hydrophobic sweetening during mammalian evolution. Rather, the fact that the residue corresponding to human TAS1R2-Y769 was serine only in species within the *Glires* clade suggests that it may have evolved toward sweetness suppression during the evolution of this clade, which includes rabbits, squirrels, and mice (Fig. 7). This study indicates that multiple fixed amino acid residues in TAS1R2-TMD are required for hydrophobic sweet compounds to be perceived as sweeteners. A comparative analysis of the TAS1R2 amino acid sequence and sweet taste sensitivity data from each animal species is required to determine the relationship between the acceptance of hydrophobic sweeteners and evolution.

In this study, the response of TAS1R2/TAS1R3 to hydrophobic low-MW compounds differed depending on the experimental system: stable single-stimulus (Fig. 1) or transient multiple-stimulus (Figs. 4 and 6). For example, in the transient multiple stimulation system, *trans*-2-hexenal showed little response (data not shown), and no significant sweet taste inhibitory effects of perillartine and cinnamaldehyde were observed. Furthermore, they were unstable throughout the HEK293 cell system, and their reactivity varied widely from day to day.

Because of these factors, it was not possible to calculate the EC_{50} and E_{max} values for each compound using dose-response curve analysis (Figure S6). Recognizing these experimental limitations, we supplemented our findings with sensory evaluations (Fig. 2) and neural response analyses (Fig. 3) to support our conclusions. Obtaining more detailed data will be the focus of future studies. The fact that *trans*-2-hexenal only causes a response at high concentrations may also explain the differences in the results between the experimental systems. The concentration of *trans*-2-hexenal required for sweetness in the sensory evaluation is approximately 5 mM, which is approximately 100 times higher than the concentration used in flavorings, making it impractical to sweeten a uniform liquid due to the overwhelming intensity of its aroma. However, given the heterogeneity of hydrophobic compounds in plants, these high concentrations are within the expected range. Plants locally accumulate fatty acids, precursors of aroma compounds, and hydrophobic compounds in oil body cells. The concentration of sesquiterpenes, which are typical aroma compounds, in oil body cells is approximately 2 mM³⁴. Therefore, it is possible that *trans*-2-hexenal localizes in agricultural products at millimolar concentrations. This suggests that if *trans*-2-hexenal can be localized in processed foods, it could evoke sweetness without generating excessively strong aromas.

Interestingly, cinnamon and shiso, which are used as spices for human food enjoyment, contain substances that taste sweet. The value of this work in taste research is highlighted by the discovery of sweetness in small volatile compounds such as *trans*-2-hexenal. Many people describe fresh fruits and vegetables as sweet when they are bitten, and this may be due not only to the sugars in the fruits and vegetables but also to the contributions of the sweet-tasting aroma compounds. The relationship between sweet aroma and the sweetness of aromatic ingredients needs to be further verified with more ingredients, since *trans*-2-hexenal and anethole have a sweet aroma, whereas vanillin, a typical sweet aroma, did not elicit a TAS1R2/TAS1R3 response. We are confident that clarification of the relationship between the aroma and taste of chemical compounds in foods will lead to a renewed concept of flavor and the creation of new flavoring methods.

Methods

Chemical compounds

Trans-2-hexenal and anethole were purchased from Inoue Perfumery, MFG, Co., Ltd. (Tokyo, Japan) as food-grade additives. Perillartine ((*E*)-4-(prop-1-en-2-yl)cyclohex-1-enecarbaldehyde oxime) was purchased from Fluorochem, Ltd. (Hadfield, UK). Cinnamaldehyde, methyl cinnamate, ethyl cinnamate, and cinnamic acid were purchased from FUJIFILM Wako Pure Chemical Corporation (Osaka, Japan). Cinnamyl alcohol and vanillin were purchased from Tokyo Chemical Industry Co., Ltd. (Tokyo, Japan). Sucralose was obtained from Sigma-Aldrich (St. Louis, MO, USA), and cyclamate was obtained from Alfa Aesar (Lancashire, UK).

Plasmid construction

Vectors expressing human *TAS1R2* and *TAS1R3* and mouse *Tas1r2* and *Tas1r3* cDNAs and the C-terminal modified G protein, *Gα16-gust44*³⁵ were previously generated^{33,36}. Chimeric *TAS1R2/Tas1r2* genes were constructed by combining human *TAS1R2* (1–564 amino acid residues) with mouse *Tas1r2* (569–844) to create human-mouse 2 (Hm2) and by combining mouse *Tas1r2* (1–568) with the human *TAS1R2* region (565–840) to create mouse-human 2 (mH2). Chimeric *TAS1R2/Tas1r2* genes were cloned into a pEF-DEST51 vector (Thermo Fisher Scientific Inc., Waltham MA). Point mutations for human *TAS1R2Y769S*, *TAS1R2L728A*, *TAS1R2T732A*, mouse *Tas1r2S773Y*, *Tas1r2L732A*, and *Tas1r2T736A* were generated by site-directed mutagenesis using human *TAS1R2* or mouse *Tas1r2* in the pEF-DEST51 vector and PrimeSTAR[®] Mutagenesis Basal Kits (Takara, Kusatsu, Japan).

Ca²⁺ imaging (stable-single stimulation system)

We performed 96-well plate Ca²⁺ flux assays using FLEX Station 3 (Molecular Devices, LLC Sunnyvale, CA, USA) in accordance with a previously described method³³. Briefly, we used the Flip-In[™] 293 cell line (Thermo Fisher Scientific, Waltham, MA, USA) for the stable expression of wild-type, chimeric, and/or point-mutated *Tas1r2/Tas1r3* with *Gα16-gust44*. Ca²⁺ flux assays were performed in cells treated with 100 μL of Hanks' Balanced Salts Solution (HBSS) containing 5 μM of the calcium indicator dye Fluo8 NW (AAT Bioquest, Sunnyvale, CA, USA). Stimulation was performed by adding 25 μL of 5 × concentrated solutions of each compound with a pipette. The intensity of the response was recorded as the relative fluorescence units (ΔRFU) value (peak value minus the value for the HBSS). Response intensity was calculated as the ratio of response to 1 mM sucralose. To determine whether the hydrophobic compounds in these experiments caused or suppressed sweetness, the Dunnett method was used to test for differences in stimulation responses with buffer alone or sucralose (1 mM) as the control group and the hydrophobic compound as the treatment group. The alpha level was set at 0.05, and the sample size was $n = 6$ according to a previous study³⁷.

Single cell Ca²⁺ imaging (transient-multi stimulation system)

Single-cell Ca²⁺ imaging was conducted, as previously described³⁸. In brief, HEK293 cells were provided by Dr. Makoto Tominaga (Thermal Biology Research Group, Nagoya Advanced Research and Development Center, Nagoya City University, Japan) and were maintained in Dulbecco's Modified Eagle Medium containing 10% fetal bovine serum at 37 °C in a humidified environment containing 5% CO₂. The cells were plated in 35-mm chambers (Ibidi, Martinsried, Germany). After 24 h of incubation, *Tas1rs* and *Gα16-gust44* (0.9 μg each) were transiently co-transfected into HEK293 cells using Lipofectamine[™] 2000 transfection reagent (Thermo Fisher Scientific, Waltham, MA, USA; 2.5 μL per 0.9 μg DNA). Twenty-four hours post-transfection, cells were incubated with 3.0 mM fluo-4 acetoxymethyl ester (Thermo Fisher Scientific) for 30 min at 37 °C. The cells were then rinsed with HBSS (Thermo Fisher Scientific) containing 10 mM 4-(2-hydroxyethyl)-1-piperazineethanesulfonic acid (HEPES; pH 7.4). Ca²⁺ imaging was then performed using a bath perfusion system. Taste solutions diluted in

HBSS containing 10 mM HEPES were sequentially applied to cells for 25 s using a peristaltic pump at a flow rate of 1.0 mL/min. Fluorescent images were captured using an S Fluor 620/0.75 objective lens (Nikon, Tokyo, Japan) and a cooled CCD camera (C6790, Hamamatsu Photonics K.K., Shizuoka, Japan) mounted on a TE300 microscope (Nikon), or a UplanXApo20x/0.80 objective lens (Olympus) via an sCMOS camera (Zyla, ANDOR, Tokyo, Japan) fitted to an IX73 microscope (Olympus). AquaCosmos 1.3 (Hamamatsu Photonics) or CellSens Dimension 4.1 (Olympus) were used for image acquisition and analysis. To prevent desensitization, a 5-min interval was maintained between the application of each tastant. Changes in intracellular Ca^{2+} concentrations were recorded in individual cells in response to stimuli (Figure S7). Cells exhibiting repeated increases in intracellular Ca^{2+} in response to sweet solutions were identified as responding cells. Changes in intracellular Ca^{2+} levels were tracked as variations in fluo-4 fluorescence. The fluorometric signals were quantified as relative fluorescence changes: $\Delta F/F_0 = (F - F_0) / F_0$, where F_0 represents the basic fluorescence level. The amplitude of Ca^{2+} changes between 5 and 25 s after the start of the stimulus was measured and averaged. Response intensity was calculated as the response ratio compared with the sucrose (1 mM). The effects of the sweet compounds were analyzed using repeated-measures one-way ANOVA, followed by post-hoc Tukey-Kramer tests. All statistical analyses were performed using GraphPad Prism version 9 (GraphPad Software, San Diego, CA, USA).

Sensory evaluation

Ethical approval for the use of human subjects was obtained from the Ethics Committee of the National Agriculture and Food Research Organization (NARO, Japan; approval number 23-H048; date of approval: February 15, 2024). The sensory tests were conducted in accordance with the Declaration of Helsinki. Eleven volunteer participants (six males and five females, aged between 23 and 49 years) were recruited from the staff members of the Institute of Food Research, NARO. All participants provided written informed consent to participate in the sensory tests. The participants could withdraw from the sensory test at any time without reason. The sensory tests were conducted in booths in an air-conditioned room ($22.3 \pm 0.2^\circ\text{C}$). The sweetness intensity of 3 solutions was evaluated: 10 mL of water, 5 mM *trans*-2-hexenal, and 50 mM sucrose. Food-grade water (Asahi Group Foods Ltd., Tokyo, Japan), sucrose (Pearl Ace Corporation, Tokyo, Japan), and *trans*-2-hexenal were used. All solutions were prepared 1 h before the sensory tests and were maintained at room temperature ($22.3 \pm 0.2^\circ\text{C}$). The solutions were presented in 2-oz plastic cups labeled with three-digit random numbers. Participants wore nose clips to minimize the effects of the aroma and placed the entire volume of the solution in each cup into their mouth. The participants confirmed the sweetness intensity of the solution for 3 s and then expectorated the solution. Sweetness intensity was rated using a 100-mm visual analog scale (VAS). The left (0) and right (100) ends of the scales were labeled with “not detectable” and “extremely strong,” which were set to the sweetness intensities of 10 mL of water and 120 mM sucrose, respectively. Salt-free crackers (Yamazaki Biscuits Co., Ltd., Tokyo, Japan) and water were used to cleanse the mouth. The solutions were served at 3-min intervals in a random order. Each solution was evaluated once. GraphPad Prism version 8 (GraphPad Software, San Diego, CA, USA) was used for statistical analyses. One-way repeated-measures ANOVA was performed on the VAS scores, with solutions as a within-subject factor at the 0.05 level. Multiple comparison tests among the solutions were conducted using the Holm–Sidak post-hoc test.

Nerve recordings

The mouse nerve recording experiments were conducted in accordance with the ARRIVE guidelines and the AVMA guidelines. Details are provided below. All experimental procedures were approved by the Committee for Laboratory Animal Care and Use at Tokyo Dental College, Japan (permit numbers: 228101 and 238101). The study subjects were adult male C57BL/6Jcl (WT) mice (CLEA Japan, Inc., Tokyo, Japan). All mice were 8–20 weeks old, weighed 20–30 g, and were maintained on a 12-h/12-h light/dark cycle.

Mice were anesthetized with an injection of a combination of anesthetic agents containing midazolam (0.8 mL/kg, Sandoz, Yamagata, Japan), medetomidine (0.75 mL/kg, Nippon Zenyaku Kogyo Co., Fukushima, Japan), butorphanol tartrate (1 mL/kg, Meiji Seika Pharma, Tokyo, Japan), and physiologic saline (7.45 mL/kg). Under anesthesia, the trachea of each mouse was cannulated, and the mouse was fixed in the supine position with a headholder to allow dissection of the taste nerves. The right CT nerve was exposed, dissected from the underlying tissues, and cut near its entrance to the bulla. The entire nerve was placed on an Ag/AgCl electrode. An indifferent electrode was placed on the surrounding tissues. Impulse discharges resulting from tongue stimulation were fed into an amplifier (LP511; Grass Amplifier, Astro-Med, West Warwick, RI, USA), integrated with a time constant of 1.0 s, and recorded on a computer for later analysis using a PowerLab system (PowerLab/sp4; AD Instruments, Australia)³⁹.

To stimulate taste by fungiform papillae (FP), the anterior half of the tongue was placed in a flow chamber. All chemicals were used at $\sim 24^\circ\text{C}$ and applied for 30 s. The tongue was washed with distilled water (DW) at 1 min or more intervals between successive stimulations to prevent desensitization. Additionally, we used 8% EtOH to wash out cinnamyl alcohol and perillartine for 10 s and checked that the response to sucralose recovered after suppression. All solutions were delivered to the tongue via gravitational flow ($\sim 0.1\text{ mL s}^{-1}$). At the end of the experiment, the animals were euthanized by intra-peritoneal injection of pentobarbital sodium (200 mg/kg). Care was taken to minimize the sufferings of animals. The taste stimuli consisted of 100 mM NH_4Cl , 100 mM NaCl, 10 mM sucralose, 300 mM monopotassium glutamate (MPG), 10 mM HCl, and 20 mM quinine HCl (QHCl). All chemicals were dissolved in DW. MPG was purchased from Merck (Darmstadt, Germany), and the other chemicals were purchased from Wako Pure Chemicals (Osaka, Japan). To block responses via TAS1R^{40–42}, each tongue was treated with $30\text{ }\mu\text{g mL}^{-1}$ ($\sim 7\text{ }\mu\text{M}$) gurmardin dissolved in 5 mM phosphate buffer (pH 6.8) for 10 min in the same manner as described by Ninomiya and Imoto⁴⁰. The cinnamyl alcohol was then dissolved in DW. Perillartine was dissolved in ethanol (EtOH) and diluted to different concentrations using DW. The final ethanol concentration was 3%.

The whole-nerve and integrated whole-nerve response magnitudes were measured from 5 to 25 s after stimulus onset. To exclude responses to 0.25, 0.75, and 1.5 mM cinnamyl alcohol or perillartine, mixed solutions of taste compounds were applied after adaptation to cinnamyl alcohol or perillartine. The mean response magnitudes were obtained subtracting mean voltages during 30 s before and after stimulation from voltages during stimulation (5–25 s after onset). Each response magnitude was normalized to responses at 100 mM NH_4Cl to account for mouse-to-mouse variations in absolute responses. The gurmardin was effective for ~20 min after washing out.

Docking simulation of perillartine to human TAS1R2/TAS1R3-TMD

Docking perillartine molecules to the potential binding sites of the human TAS1R2/TAS1R3-transmembrane domain (TMD) involved four steps: (1) structure preparation of the human TAS1R2/TAS1R3-TMD, (2) binding site prediction, (3) docking of perillartine molecules, and (4) molecular dynamics simulation of post-docking processing. The monomeric structures of human TAS1R2 and TAS1R3 were obtained from the AlphaFold2 database⁴³, and their extracellular domains (1–544 of TAS1R2 and 1–547 of TAS1R3) were truncated. The human TAS1R2/TAS1R3-TMD complex model was constructed using CaSR structural information (PDB-ID: 7 m3g) as a template. The TAS1R2 and TAS1R3 structures are superimposed on the A and B chains of CaSR, respectively. The proposed human TAS1R2/TAS1R3-TMD model was refined for docking simulations using the Protein Preparation Wizard Script in Maestro (Schrödinger, LLC, New York, NY, USA). Based on the results of the chimeric mutant experiments, putative druggable sites on human TAS1R2 were detected and represented by small dummy atoms using grid-based energy calculations^{44,45} incorporated in the SiteMap program (Schrödinger, LLC, New York, NY, USA). For perillartine molecules, ionization and energy minimization were performed using the OPLS3 force field in the LigPrep Script in Maestro (Schrödinger, LLC, New York, NY, USA). Docking simulations of perillartine with human TAS1R2-TMD were performed using the Glide^{46,47}, the SP docking program (Schrödinger LLC, New York, NY, USA). The best docking score pose was subjected to five independent MD simulations with different initial velocities for each target using Desmond version 2.3 (Schrödinger, LLC, New York, NY, USA) for post-docking processing. The OPLS3e force field^{48,49} was used in the simulations. Initial model structures were placed into a large POPC bilayer and TIP3P water molecules with periodic boundary conditions using an orthorhombic 10 Å layer simulation box. The system was neutralized, and an ionic force of 0.15 M was set by adding Na^+ and Cl^- ions. After minimization and relaxation of the model, the MD production phase was performed for 200 ns with a time step of 2 fs in an isothermal–isobaric (NPT) ensemble at 300 K and 1 bar using a Langevin thermostat. The long-range electrostatic interactions were computed using the Smooth Particle Mesh Ewald method⁵⁰. The MD trajectories were saved every 10 ps for analysis. All system setups were performed using Maestro software (Schrödinger LLC, New York, NY, USA). Protein–ligand interaction fingerprint (PLIF) analyses from MD trajectories were also performed using the PLIF modules of MOE 2020.0901 (Chemical Computing Group Inc., Montreal, Quebec, Canada). After the PLIFs were generated based on the 5000 snapshot structures (every 10 ps from the last 100 ns in five independent 200 ns simulation) for the perillartine molecule, the population histogram of contacts for each residue around perillartine was calculated. The docking procedure for mouse TAS1R2/TAS1R3 was identical to that used humans.

Data availability

The datasets supporting the conclusions of this study are available from the NARO-Linked DB maintained by the National Agriculture and Food Research Organization (not yet released, available upon request). The corresponding author should be contacted to request access to the datasets.

Received: 6 August 2024; Accepted: 7 February 2025

Published online: 12 March 2025

References

1. *Handbook of Food Chemistry* (Springer, 2015).
2. Nelson, G. et al. Mammalian sweet taste receptors. *Cell* **106**, 381–390 (2001).
3. Nelson, G. et al. An amino-acid taste receptor. *Nature* **416**, 199–202 (2002).
4. Pin, J. P., Galvez, T. & Prézeau, L. Evolution, structure, and activation mechanism of family 3/C G-protein-coupled receptors. *Pharmacol. Ther.* **98**, 325–354 (2003).
5. Jiang, P. et al. Identification of the cyclamate interaction site within the transmembrane domain of the human sweet taste receptor subunit Tas1r3. *J. Biol. Chem.* **280**, 34296–34305 (2005).
6. Jiang, P. et al. Lactisole interacts with the transmembrane domains of human T1R3 to inhibit sweet taste. *J. Biol. Chem.* **280**, 15238–15246 (2005).
7. Sanematsu, K. et al. Molecular mechanisms for sweet-suppressing effect of gymnemic acids. *J. Biol. Chem.* **289**, 25711–25720 (2014).
8. Zhang, F. et al. Molecular mechanism for the umami taste synergism. *Proc. Natl. Acad. Sci. U S A.* **105**, 20930–20934 (2008).
9. Cravotto, G., Nano, G. M., Binello, A., Spagliardi, P. & Seu, G. Chemical and biological modification of cynaropicrin and grosheimin: a structure–bitterness relationship study. *J. Sci. Food Agric.* **85**, 1757–1764 (2005).
10. Munk, C. et al. GPCRdb: the G protein-coupled receptor database – an introduction. *Br. J. Pharmacol.* **173**, 2195–2207 (2016).
11. Scotti, L. et al. Quantitative elucidation of the structure–bitterness relationship of cynaropicrin and grosheimin derivatives. *Food Chem.* **105**, 77–83 (2007).
12. Cho, M. J., Unklesbay, N., Hsieh, F. H. & Clarke, A. D. Hydrophobicity of bitter peptides from soy protein hydrolysates. *J. Agric. Food Chem.* **52**, 5895–5901 (2004).
13. Hussain, R. A., Poveda, L. J., Pezzuto, J. M., Soejarto, D. D. & Kinghorn, A. D. Sweetening agents of plant origin: phenylpropanoid constituents of seven sweet-tasting plants. *Econ. Bot.* **44**, 174–182 (1990).
14. Yokomi, N. & Ito, M. Influence of composition upon the variety of tastes in Cinnamomi Cortex. *J. Nat. Med.* **63**, 261–266 (2009).

15. Cai, C. et al. Characterization of the sweet taste receptor Tas1r2 from an Old World monkey species rhesus monkey and species-dependent activation of the monomeric receptor by an intense sweetener perillartine. *PLoS ONE*. **11**, e0160079 (2016).
16. Toda, Y. et al. Positive/negative allosteric modulation switching in an umami taste receptor (T1R1/T1R3) by a natural flavor compound, methional. *Sci. Rep.* **8**, 11796 (2018).
17. Atkinson, R. G. Phenylpropenes: Occurrence, distribution, and biosynthesis in fruit. *J. Agric. Food Chem.* **66**, 2259–2272 (2018).
18. Bandell, M. et al. Noxious cold ion channel TRPA1 is activated by pungent compounds and bradykinin. *Neuron* **41**, 849–857 (2004).
19. Talavera, K. et al. Mammalian TRPA1: From structure to disease running title: Mammalian TRPA1 : From structure to disease keywords : Transient receptor potential – Ca 2+ channel - nociception - chemosensation - thermosensation - mechanosensation - channelopathies - pain (2019).
20. Blair, N. T. et al. Naturally produced defensive alkenal compounds activate TRPA1. *Chem. Senses*. **41**, 281–292 (2016).
21. Hellekant, G. & Danilova, V. Species differences toward sweeteners. *Food Chem.* **56**, 323–328 (1996).
22. Nofre, C., Tinti, J. M. & Glaser, D. Evolution of the sweetener receptor in primates. II. Gustatory responses of non-human primates to nine compounds known to be sweet in man. *Chem. Senses*. **21**, 747–762 (1996).
23. Glaser, D., Hellekant, G., Brouwer, J. N. & Van Der Wel, H. Effects of gymnemic acid on sweet taste perception in primates. *Chem. Senses*. **8**, 367–374 (1984).
24. Chéron, J. B., Golebiowski, J., Antonczak, S. & Fiorucci, S. The anatomy of mammalian sweet taste receptors. *Proteins* **85**, 332–341 (2017).
25. Zhao, M., Xu, X. Q., Meng, X. Y. & Liu, B. The heptahelical domain of the sweet taste receptor Tas1r2 is a new allosteric binding site for the sweet taste modulator amiloride that modulates sweet taste in a species-dependent manner. *J. Mol. Neurosci.* **66**, 207–213 (2018).
26. Imoto, T., Miyasaka, A., Ishima, R. & Akasaka, K. A novel peptide isolated from the leaves of *Gymnema sylvestre*-I. characterization and its suppressive effect on the neural responses to sweet taste stimuli in the rat. *Comp. Biochem. Physiol. Comp. Physiol.* **100**, 309–314 (1991).
27. Gilbertson, T. A., Roper, S. D. & Kinnamon, S. C. Proton currents through amiloride-sensitive Na⁺ channels in isolated hamster taste cells: enhancement by vasopressin and cAMP. *Neuron* **10**, 931–942 (1993).
28. Nie, Y., Vignes, S., Hobbs, J. R., Conn, G. L. & Munger, S. D. Distinct contributions of Tas1r2 and Tas1r3 taste receptor subunits to the detection of sweet stimuli. *Curr. Biol.* **15**, 1948–1952 (2005).
29. Masuda, K. et al. Characterization of the modes of binding between human sweet taste receptor and low-molecular-weight sweet compounds. *PLoS ONE*. **7**, e35380 (2012).
30. Winnig, M., Bufer, B., Kratochwil, N. A., Slack, J. P. & Meyerhof, W. The binding site for neohesperidin dihydrochalcone at the human sweet taste receptor. *BMC Struct. Biol.* **7**, 66 (2007).
31. Nakagita, T. et al. Ibuprofen, a nonsteroidal anti-inflammatory drug, is a potent inhibitor of the human sweet taste receptor. *Chem. Senses*. **45**, 667–673 (2020).
32. Pérez-Benito, L. et al. Molecular switches of allosteric modulation of the metabotropic glutamate 2 receptor. *Structure* **25**, 1153–1162e4 (2017).
33. Shimizu, M., Goto, M., Kawai, T., Yamashita, A. & Kusakabe, Y. Distinct human and mouse membrane trafficking systems for sweet taste receptors Tas1r2 and Tas1r3. *PLoS ONE*. **9**, e100425 (2014).
34. Tanaka, M. et al. Direct evidence of specific localization of sesquiterpenes and marchantin A in oil body cells of *Marchantia polymorpha* L. *Phytochemistry* **130**, 77–84 (2016).
35. Ueda, T., Ugawa, S., Yamamura, H., Imaizumi, Y. & Shimada, S. Functional interaction between T2R taste receptors and G-protein α subunits expressed in taste receptor cells. *J. Neurosci.* **23**, 7376–7380 (2003).
36. Kusakabe, Y., Shindo, Y., Kawai, T., Maeda-Yamamoto, M. & Wada, Y. Relationships between the response of the sweet taste receptor, salivation toward sweeteners, and sweetness intensity. *Food Sci. Nutr.* **9**, 719–727 (2021).
37. Ogawa, Y., Zhou, L., Kaneko, S. & Kusakabe, Y. Agonistic/antagonistic properties of lactones in food flavors on the sensory ion channels TRPV1 and TRPA1. *Chem. Senses*. **47**, 1–10 (2022).
38. Sanematsu, K. et al. Prediction of dynamic allostery for the transmembrane domain of the sweet taste receptor subunit, Tas1r3. *Commun. Biol.* **6**, 340 (2023).
39. Yasumatsu, K. et al. Involvement of multiple taste receptors in umami taste: analysis of gustatory nerve responses in metabotropic glutamate receptor 4 knockout mice. *J. Physiol.* **593**, 1021–1034 (2015).
40. Ninomiya, Y. & Imoto, T. Gurmardin inhibition of sweet taste responses in mice. *Am. J. Physiol.* **268**, R1019–R1025 (1995).
41. Margolskee, R. F. et al. T1R3 and gustducin in gut sense sugars to regulate expression of Na⁺-glucose cotransporter 1. *Proc. Natl. Acad. Sci. U. S. A.* **104**, 15075–15080 (2007).
42. Daly, K. et al. Sensing of amino acids by the gut-expressed taste receptor T1R1-T1R3 stimulates CCK secretion. *Am. J. Physiol. Gastrointest. Liver Physiol.* **304**, G271–G282 (2013).
43. Tunyasuvunakool, K. et al. Highly accurate protein structure prediction for the human proteome. *Nature* **596**, 590–596 (2021).
44. Halgren, T. New method for fast and accurate binding-site identification and analysis. *Chem. Biol. Drug Des.* **69**, 146–148 (2007).
45. Halgren, T. A. Identifying and characterizing binding sites and assessing druggability. *J. Chem. Inf. Model.* **49**, 377–389 (2009).
46. Friesner, R. A. et al. Glide: a new approach for rapid, accurate docking and scoring. 1. Method and assessment of docking accuracy. *J. Med. Chem.* **47**, 1739–1749 (2004).
47. Halgren, T. A. et al. Glide: A new approach for rapid, accurate docking and scoring. 2. Enrichment factors in database screening. *J. Med. Chem.* **47**, 1750–1759 (2004). Glide.
48. Roos, K. et al. OPLS3e: extending force field coverage for drug-like small molecules. *J. Chem. Theor. Comput.* **15**, 1863–1874 (2019).
49. Kurki, M., Poso, A., Bartos, P. & Miettinen, M. S. Structure of POPC lipid bilayers in OPLS3e force field. *J. Chem. Inf. Model.* **62**, 6462–6474 (2022).
50. Essmann, U. et al. A smooth particle mesh Ewald method. *J. Chem. Phys.* **103**, 8577–8593 (1995).

Acknowledgements

This work was supported by JSPS KAKENHI (grant number JP24K08760 to YK., KS., and KY) and Tokyo Dental College Research (grant for the Well-being Project to KY).

Author contributions

YK conceived the study. YK, TH, and AY conceptualized the study, and YK, NS, and AY supervised the study. FH, KS, KY, NS, TH, and YK designed the experiments. YK and KS performed cell response analysis. FH performed the sensory evaluations. KY performed the neural response analysis. TH performed docking simulations. FH, KS, KY, TH, AY, and YK interpreted the data. FH, KS, KY, TH, and YK wrote the manuscript. All authors have read and approved the final version of the manuscript.

Declarations

Competing interests

The authors declare no competing interests.
The authors declare no competing interests.

Additional information

Supplementary Information The online version contains supplementary material available at <https://doi.org/10.1038/s41598-025-89711-9>.

Correspondence and requests for materials should be addressed to Y.K.

Reprints and permissions information is available at www.nature.com/reprints.

Publisher's note Springer Nature remains neutral with regard to jurisdictional claims in published maps and institutional affiliations.

Open Access This article is licensed under a Creative Commons Attribution-NonCommercial-NoDerivatives 4.0 International License, which permits any non-commercial use, sharing, distribution and reproduction in any medium or format, as long as you give appropriate credit to the original author(s) and the source, provide a link to the Creative Commons licence, and indicate if you modified the licensed material. You do not have permission under this licence to share adapted material derived from this article or parts of it. The images or other third party material in this article are included in the article's Creative Commons licence, unless indicated otherwise in a credit line to the material. If material is not included in the article's Creative Commons licence and your intended use is not permitted by statutory regulation or exceeds the permitted use, you will need to obtain permission directly from the copyright holder. To view a copy of this licence, visit <http://creativecommons.org/licenses/by-nc-nd/4.0/>.

© The Author(s) 2025